Biosensors and Bioelectronics 106 (2018) 57–63

Contents lists available at ScienceDirect

Biosensors and Bioelectronics

journal homepage: www.elsevier.com/locate/bios

A sensitive Potentiometric resolved ratiometric Photoelectrochemical aptasensor for Escherichia coli detection fabricated with non-metallic nanomaterials

Rong Hua, Nan Hao*, Jinwen Lu, Jing Qian, Qian Liu, Henan Li, Kun Wang*

School of Chemistry and Chemical Engineering, Jiangsu University, Zhenjiang 212013, PR China

ARTICLE INFO

Keywords:
Ratiometric sensing
Photoelectrochemical biosensor
Nonmetallic materials
Escherichia coli

ABSTRACT

In this work, a sensitive potentiometric resolved ratiometric photoelectrochemical aptasensor for Escherichia coli (*E. coli*) detection was successfully fabricated with non-metallic nanomaterials. To avoid the use of precious metals or heavy metals, three-dimensional graphene hydrogel-loaded carbon quantum dots (C-dots/3DGH) and graphene-like carbon nitride (g-C_3N_4) with excellent PEC activity and matched potential were prepared. These two materials were modified onto two adjacent areas on the ITO electrode. By applying different bias voltage, the cathodic current generated by C-dots/3DGH and the anodic current generated by g-C_3N_4 can be clearly distinguished and would not interfere with one another. Then *E. coli* aptamer was modified onto the surface of C-dots/3DGH. In the presence of targets, the binding of *E. coli* with aptamer lead to the steric hindrance greatly increased and the cathodic current decreased significantly. Meanwhile, the anodic current generated by g-C_3N_4 was not influenced and it can serve as a stable reference to evaluate the environmental factors. Therefore, the concentration of *E. coli* can be quantified by the ratio of cathodic current to anodic current, which can effectively eliminate these analyte-independent factors and provide a more precise analysis. In addition, this ratiometric PEC biosensor also showed a good sensitivity and a wide linear range (2.9 cfu/mL to 2.9 × 10^6 cfu/mL).

1. Introduction

As a representative foodborne pathogen, Escherichia coli (*E. coli*) is usually infected by consuming unprocessed or contaminated food and can lead to the outbreak of large-scale infectious diseases (Deisingh and Thompson, 2004), which is a great threat to human health. However, traditional foodborne pathogen detection methods, such as microscopic culture (Siegmund et al., 2013) and polymerase chain reaction (Lawal et al., 2015), are costly and need a long processing time, which cannot satisfy the demands from food safety monitoring and clinical diagnosis. Thereby it is very necessary to develop a fast, simple and sensitive method for *E. coli* detection.

Photoelectrochemistry (PEC) phenomenon refers to a process that the photosensitive material absorbed photons to produce electron-hole pairs and then caused the oxidation-reduction reaction at the interface. In recent year, based on the combination of photoelectrochemistry and traditional electrochemical sensing, PEC sensing technology has rapidly attracted the attention of researchers (Li et al., 2016a; Moakhar et al., 2015; Xu et al., 2017; Zhang et al., 2016; Zhao et al., 2017). Compared with traditional optical methods, PEC detector equipment is simple, low price and easy to miniaturize (Golub et al., 2009; Li et al., 2011) because of the use of electrical signal output (Zhao et al., 2014). Besides the advantages of low cost and simple instrumentation, PEC sensing also has a better sensitivity due to the separation of excitation source (optical signal) and detection signal (electrical signal), which provides a lower background signal and the detection limit can be further reduced (Wang et al., 2009). The relevant experiments demonstrated that the detection limit obtained by the PEC method is usually one order of magnitude lower than conventional electrochemical methods when using the same or similar process (Zhao et al., 2015). It has shown a huge advantage in environmental monitoring, food safety, especially in the field of bioanalysis. A variety of PEC biosensors have been developed to detect the corresponding target on account of different biometric elements. The quantitative detection of the photoelectric sensor usually depends on the change in the intensity of the photocurrent caused by the reaction between the target and the optoelectronic active material or the bio-probe (Li et al., 2016b). However, the photocurrent may be interfered by the environmental factors. Ratiometric sensing is an effective tool to improve the detection reliability and have been widely applied in fluorescence detection (Zhang et al., 2011, 2008; Zhu

* Corresponding authors.
E-mail addresses: hn@ujs.edu.cn (N. Hao), wangkun@ujs.edu.cn (K. Wang).

https://doi.org/10.1016/j.bios.2018.01.053
Received 11 December 2017; Received in revised form 20 January 2018; Accepted 24 January 2018

et al., 2017) and electrochemical sensors (Hussein et al., 2017; Feng et al., 2016; Wang et al., 2016). Yet, so far, there is few reports about PEC ratiometric sensing because it is more difficult to distinguish photocurrents from different PEC active material. In a recent research, we have successfully developed a novel potentiometric resolved ratiometric PEC aptasensor (Zhang et al., 2017). By applying different bias voltage, the cathodic current and anodic current from two PEC active materials can be generated in order and would not interfere with one another. The quantification of targets was achieved based on the ratiometric between cathodic current and anodic current, which can effectively reduce the external factors interference on the detection results and improve the accuracy of the photoelectric detection process. Meanwhile, this method can be easily operated with present PEC systems and has no additional instrument requirement, providing a simple and common ratiometric PEC detection approach.

Various nonmetallic PEC active nanomaterials, such as carbon dots (Tan et al., 2017; Tiwari et al., 2017) and carbon nitride (She et al., 2016; Zou et al., 2017), have been paid great attention in recent years. Compared with traditional semiconductor materials, nonmetallic nanomaterials are undoubtedly more environmental friendly and can effectively reduce the potential toxicity both to health and environment. In this study, three-dimensional graphene hydrogel-loaded carbon quantum dots (C-dots/3DGH) and graphene-like carbon nitride (g-C_3N_4) with excellent PEC activity and matched potential were prepared to construct a highly sensitive ratiometric PEC biosensor for *E. coli* detection. Besides a better reliability, this proposed biosensor also exhibited a good performance with a wide linear range from 2.9 to 2.9 × 10^6 cfu/mL with an extremely low detection limit of 0.66 cfu/mL (S/N = 3).

2. Experimental

2.1. Reagents and chemicals

Graphite was purchased from Qingdao Tianhe Graphite Co., Ltd (Qingdao, China). Amino-functionalized aptamer was obtained from Sangon Biotech Co., Ltd (Shanghai, China) and the sequence as following:5′-GCA ATG GTA CGG TAC TTC CCC ATG AGT GTT GTG AAA TGT TGG GAC ACT AGG TGG CAT AGA GCC GCA AAA GTG CAC GCT ACT TTG CTA A-3′-NH_2-$(CH_2)_6$. 1-ethyl-3-(3-dimethylaminopropyl) carbodiimide hydrochloride (EDC), N-Hydroxysuccinimide (NHS), chitosan(CS), glucose and bovine serum albumin (BSA) were provided from Sigma-Aldrich Co. (St. Louis, MO, USA). Furthermore, other reagents and chemicals were obtained from Sinopharm Chemical Reagent Co., Ltd. Phosphate buffer solutions (PBS, 0.1 M) were prepared from NaOH, Na_2HPO_4, and NaH_2PO_4. Graphene oxide (GO) was prepared using modified Hummers method from graphite powders (Gilje et al., 2007). All other chemicals were of analytical grade, and the aqueous solutions were prepared with doubly distilled water.

2.2. Apparatus

The morphologies of the samples were determined using a H800 transmission electron microscope (TEM, Hitachi, Japan). Crystal structure identification was determined using X-ray diffraction (XRD) with a D8 diffractometer (Bruker, Germany) with high-intensity Cu Kα (λ = 1.5406 Å) radiation. Raman spectra were carried out on an RM 2000 microscopic confocal Raman spectrometer. The FT-IR characterizations of the samples were analyzed with Nicolet Nexus 470FT-I FT-IR spectrometer. All the electrochemical and PEC measurements were performed with a CHI 660B electrochemical workstation (Chen Hua Instruments Co., Shanghai, China) and recorded by a conventional three-electrode system where an indium tin oxide (ITO) as a working electrode, a saturated calomel electrode (SCE) as a reference electrode, and a platinum (Pt) wire as a counter electrode. PEC measurement was carried out in 0.1 M phosphate buffer solution (PBS) at critical voltage and a 500 W Xe lamp (Beijing Chang Tuo) was used as the visible light source with 400-nm cut-off filter placed into the path of the Xe lamp to remove the UV irradiation. The synthesis of carbon nitride was accomplished by using a high temperature furnace (Hefei Ke Jing Materials Technology Co., Ltd.) as well as an ultrasonic machine (Kunshan Ultrasonic Instruments Co., Ltd.).

2.3. Preparation of materials

2.3.1. Three-dimensional graphene hydrogel-loaded carbon quantum dots (C-dots/3DGH) were synthesized as following

Firstly, 300 mg glucose was dissolved in 10 mL graphene oxide (2 mg/mL) to form a homogeneous solution. Then, as-prepared solution was transferred into a Teflon-scaled autoclave as well as heated at 180 °C for 12 h and then cooled to room temperature naturally to generate C-dots/3DGH. Finally, the obtained C-dots/3DGH nanocomposites were washed and freeze dried for 48 h.

2.3.2. The g-C_3N_4 was prepared according to the previously published method (Amiri et al., 2016; Amouzadeh Tabrizi et al., 2017) as follows

In short, 2.0 g melamine powder was transferred into high temperature furnace and heated at 520 °C for 4.0 h under argon condition with a ramp rate of about 3 °C/min. The obtained yellow powder was grounded and used for further characterizations (Supplementary materials, the typical SEM image shown in Fig. S1 A, and the XRD patterns as well as FT-IR spectra of g-C_3N_4 were also presented in Fig. S2. These results were demonstrated the successful preparation of graphitic carbonitride.). At last, 5 mg of g-C_3N_4 was dispersed in 1 mL of isopropanol alcohol with ultrasonic agitation for 2 h to achieve a well-dispersed suspension.

2.3.3. Fabrication of the ratiometric PEC Aptasensor

The ITO glass (1 cm × 3 cm) was cleaned with sonication in water and ethanol, respectively. Furthermore, it was dried under an infrared light. Then, the two previously prepared materials C-dots/3DGH and g-C_3N_4 were modified onto two adjacent areas on the ITO electrode. On one side, about 20 μL of C-dots/3DGH (2 mg/mL) was dropped onto the pretreated ITO and dried in air for an hour. Next, 20 μL of EDC and NHS were respectively added dropwise to the ITO electrode surface (Settu et al., 2017), and, allowed to stand for 50 min to activate the carboxyl group (Han et al., 2015). Then, it was washed by ultrapure water and dried in air. Afterward, 20 μL of 1 μM aptamers were coated on the surface of modified electrode at 4 °C for 12 h and then the unreacted aptamers were washed by buffer solution (pH = 7.4). Finally, 20 μL of 1% BSA was coated on the electrode for an hour to block remaining active sites and then was washed with PBS buffer solution for several times (Li et al., 2017; Qian et al., 2010). On the other side, about 20 μL of g-C_3N_4 (1.5 mg/mL) was dropped onto the pretreated ITO and dried in air for an hour. The obtained ratiometric PEC aptasensor was stored at 4 °C.

2.4. Bacterial strain culturing and plate counting

Bacterial suspension of *E. coli* was cultivated in Luria-Bertani at 37 °C with shaking (250 rpm) for 16 h. Then 1 mL bacterial liquid was taken for the detection of absorbance (wavelength of 600 nm). Next, to study the activity of *E. coli*, 1 mL of the bacterial liquid was removed from the tube for 10-fold successively diluted in PBS solution, and 200 μL of each plated on LB agar plates which were cultivated at 37 °C for 36 h. At last, the number of colony-forming units per milliliter (cfu/mL) could be obtained by counting the colonies of *E.coli* on the plate (Hao et al., 2017a).

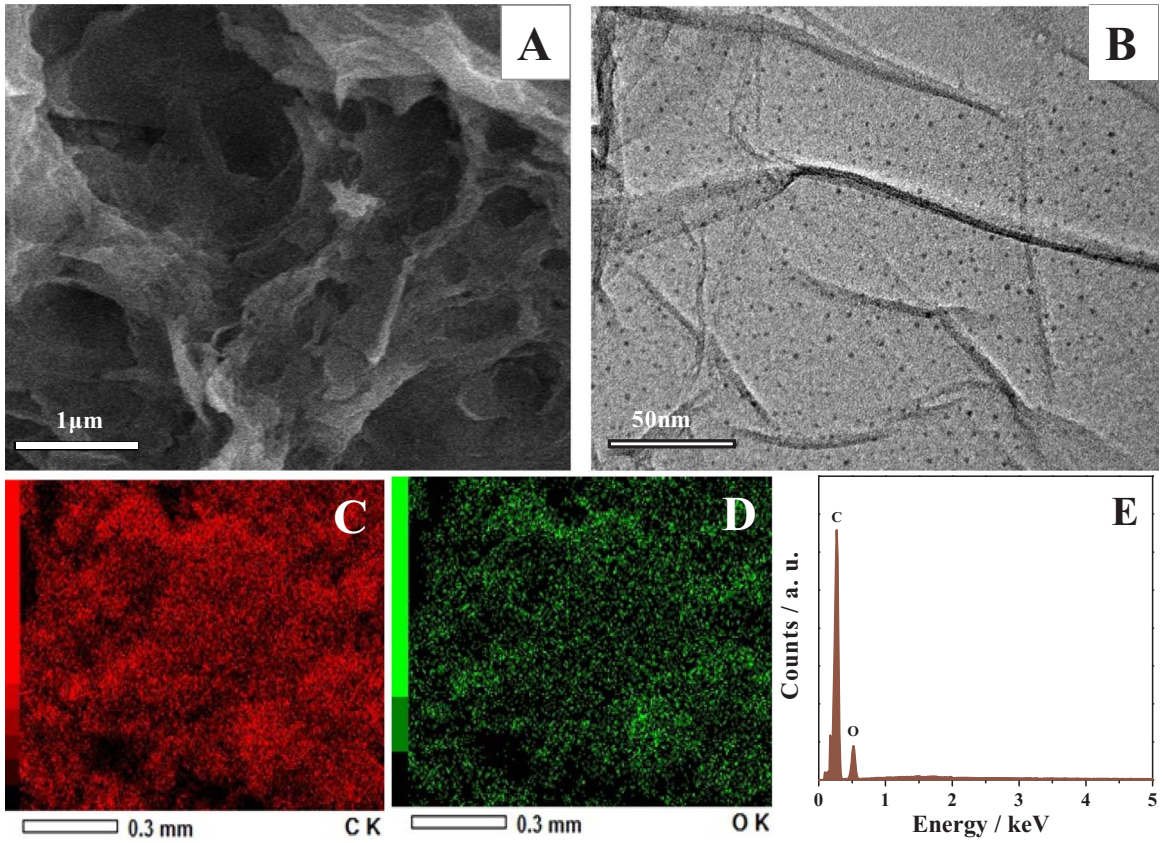

Fig. 1. The typical SEM images of C-dots/3DGH nanocomposites (A). The TEM images of C-dots/3DGH nanocomposites (B) Elemental mapping images (EMIs) of C (C) and O (D) of C-dots/3DGH nanocomposites. (E) EDS of C-dots/3DGH nanocomposites obtained from SEM.

3. Results and discussion

3.1. Characterization of synthesized nanomaterials

The structure and morphology of the as-prepared nanocomposites have been carefully investigated through a variety of characterization methods. As shown in Fig. 1 A, the surface scanning electron microscopy (SEM) image revealed that the three-dimensional graphene hydrogel-loaded carbon dots nanocomposites exhibited a well cross-linked porous structure. The TEM image of three-dimensional graphene hydrogel (3DGH) showed that the material had a pleated flake structure (Fig. S1B). In contrast to pure 3DGH, the image of transmission electron microscope (Fig. 1B) revealed that the average diameter of carbon dots is around 5 nm, which were homogeneously loaded on the surface of the three-dimensional graphene hydrogel. These results demonstrated that the successful preparation of three-dimensional graphene hydrogel-loaded carbon dots nanocomposites. In addition, elemental mapping images (EMIs) indicated the existence of C and O elements (Fig. 1C-D), the corresponding energy dispersive spectroscopy (EDS) spectrum also demonstrated the existence of C and O in the composite (Fig. 1E).

Fig. 2A exhibited X-ray diffraction (XRD) patterns of 3DGH (a), C-dots/3DGH nanocomposites (b) respectively. From the patterns, the broadened characteristic peak of graphene at 24.3° (002) was observed. It also displayed a broad diffraction peak at 43.2°, corresponding to the (100) plane of graphene (Lin et al., 2017). Moreover, the peak intensity of curve b was stronger than curve a, which indicated that the crystallinity of the C-dots/3DGH nanocomposites was larger than that of the 3DGH. It is widely known that Raman spectroscopy is a technique that the most directly and nondestructively characterize the structure of the

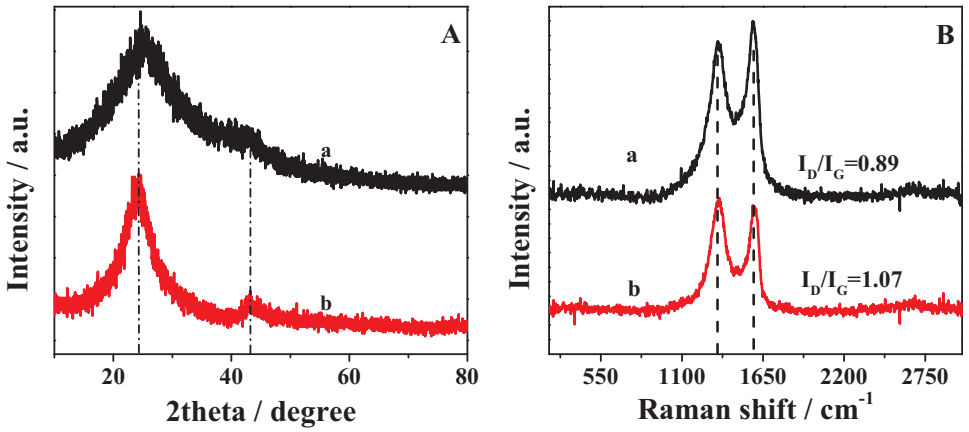

Fig. 2. (A) XRD patterns of 3DGH (a), C-dots/3DGH nanocomposites (b) and (B) Raman spectra of 3DGH (a), C-dots/3DGH nanocomposites (b).

carbon materials, particularly to study the ordered, disordered and defects of graphene materials. As shown in Fig. 2B, two prominent peaks located ~ 1342 cm^{-1} and ~ 1583 cm^{-1} in Raman spectroscopy are due to the D-band and G-band of graphene (Hao et al., 2017b; Kang et al., 2017), the D-band was related to defects and grading disorder in the bent graphene flakes, while the G-band represented the graphite hexagonal clamping mode. Obviously, the peak intensity ratio of D to G band of C-dots/3DGH nanocomposites (I_D/I_G = 1.07, curve b) was greater than pure 3DGH (I_D/I_G = 0.89, curve a), which revealed that C-dots/3DGH nanocomposites with the larger crystal defects that was in accordance to the results of X-ray diffraction (XRD) patterns.

Meanwhile, the FT-IR spectrum was performed to investigate the functional groups of 3DGH and C-dots/3DGH nanocomposites. As shown in Fig. S3 curve a, owing to the stretching vibration absorption of -OH (which was mainly due to the adsorption of water molecules in the sample), a wide and strong absorption peak appeared at 3271 cm^{-1}. The stretching (carbonyl C=O) and the skeleton (C=C) vibration absorption peak appeared at 1762 cm^{-1} and 1614 cm^{-1}, respectively. Besides, a peak appeared at 1049 cm^{-1} which was the bending vibration absorption peak of C-O (Zhang et al., 2018). Curve b displayed three peaks at 3298, 1654 as well as 1540 cm^{-1},which are attributed to the stretching vibration of C–OH, C=O and C–C bonds, respectively (Yogesh et al., 2017). In addition, two distinct peaks appeared at 1246 and 1055 cm^{-1} because of the stretching vibration of C-O at different positions in the structure. Compared curve a and curve b, the peak of stretching vibration of C=O and C–C bonds of C-dots/3DGH nanocomposites were much stronger than that of 3DGH. Therefore, the FTIR results confirmed that C-dots/3DGH nanocomposites were modified with abundant carboxylic functional groups.

3.2. Experimental mechanism

In this work, two nonmetal materials C-dots/3DGH and g-C_3N_4 were introduced into ratiometric PEC sensing system. Scheme 1. illustrated the principle of this ratiometric PEC sensor. First, two prepared materials were modified respectively on two adjacent areas of the ITO electrode surface. Then, when the bias voltage was set to 0.15 V , which was the critical voltage of g-C_3N_4 under light irradiation, the photocurrent from g-C_3N_4 was zero. And the obtained photocurrent of this ITO electrode was completely generated by C-dots/3DGH. When the bias voltage was switched from 0.15 V to −0.4 V (the critical voltage of C-dots/3DGH), the corresponding photocurrent then changed from the cathodic current (generated by C-dots/3DGH) to the anodic current (generated by g-C_3N_4). Then *E. coli* aptamer was modified onto the surface of C-dots/3DGH and BSA was applied to block active sites. The cathodic current at 0.15 V was reduced because of the increased steric hindrance. In the presence of *E. coli*, the binding of *E. coli* with aptamer lead to the steric hindrance greatly increased and the cathodic current at 0.15 V decreased significantly. Meanwhile, the anodic current generated by g-C_3N_4 was not influenced in the whole process and it can serve as a stable reference to evaluate the environmental factors. The concentration of *E. coli* can be quantified by the ratiometric between cathodic current and anodic current, which can effectively eliminate these analyte-independent factors and provide a more precise analysis.

3.3. The optimization of experimental conditions

In order to achieve the optimal PEC response for Escherichia coli determination, the relevant factors on the PEC performance was investigated. For the aptamer modification, the PEC intensity decreased with increasing the aptamer concentration and reached a plateau around 1.0 μM (Fig. S4A). In addition, the incubation time of the aptamer and the binding time with *E. coli* were also optimized. As displayed in Fig. S4B, with the increase of incubation time, the intensity of photocurrent gradually decreased. When the aptamer was incubated for 12 h, the photocurrent intensity gradually stabilized. The effect of temperature (Fig. S4C) on the PEC performance was also investigated. As shown in Fig. S4C, the PEC intensity decreased with increasing temperature, and while the temperature was 37 °C, the PEC intensity was slowly leveled off. Similarly, the intensity of photocurrent gradually decreased with the binding time of the target increased and did not change much after 40 min (Fig. S4D). Thus, 1.0 μM aptamer was chosen as the optimum concentration, 37 °C was selected as the optimum binding temperature of *E. coli* with aptamer. 12 h and 40 min was used as the optimum incubation time of aptamer and the optimum binding time of *E. coli* with the aptamer, respectively, in this study.

3.4. The detection of Escherichia coli based on PEC ratiometric sensing

At first, the PEC performances of g-C_3N_4 and C-dots/3DGH under light illumination with different bias voltage was investigated, respectively. As shown in Fig. 3A, the curves from left to right represented the photocurrent intensity of g-C_3N_4 at 0 V, 0.05 V, 0.1 V, 0.15 V, 0.2 V, 0.25 V, respectively. Likewise, the photocurrent intensity of C-dots/3DGH at 0 V, 0.05 V, 0.1 V, 0.15 V, 0.2 V, 0.25 V were presented in Fig. 3B. It was obvious that the value and polarity of the photocurrents were influenced by the applied voltage changes. And the critical

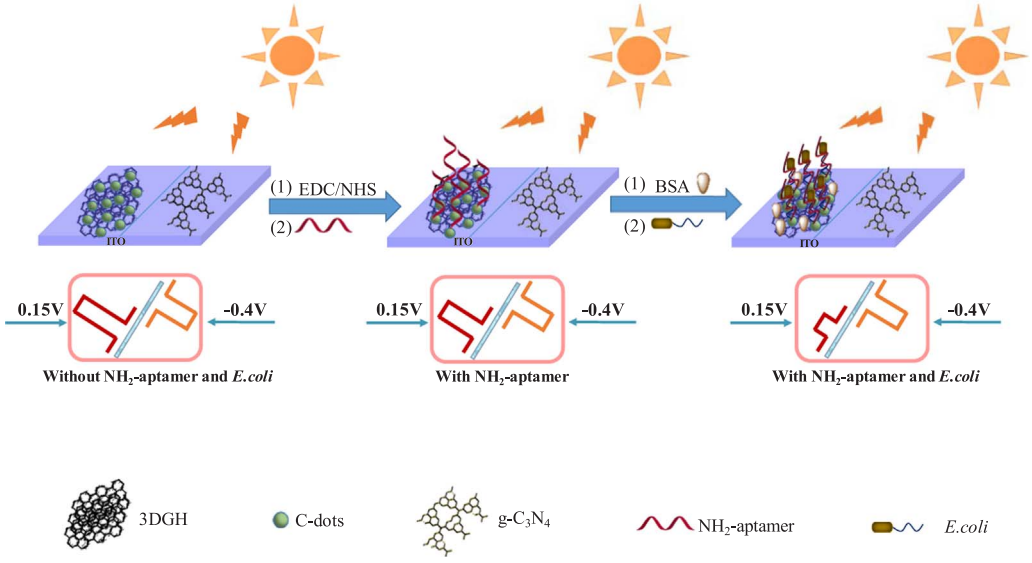

Scheme 1. Schematic diagram for the detection of *E. coli* with the ratiometric PEC aptasensor.

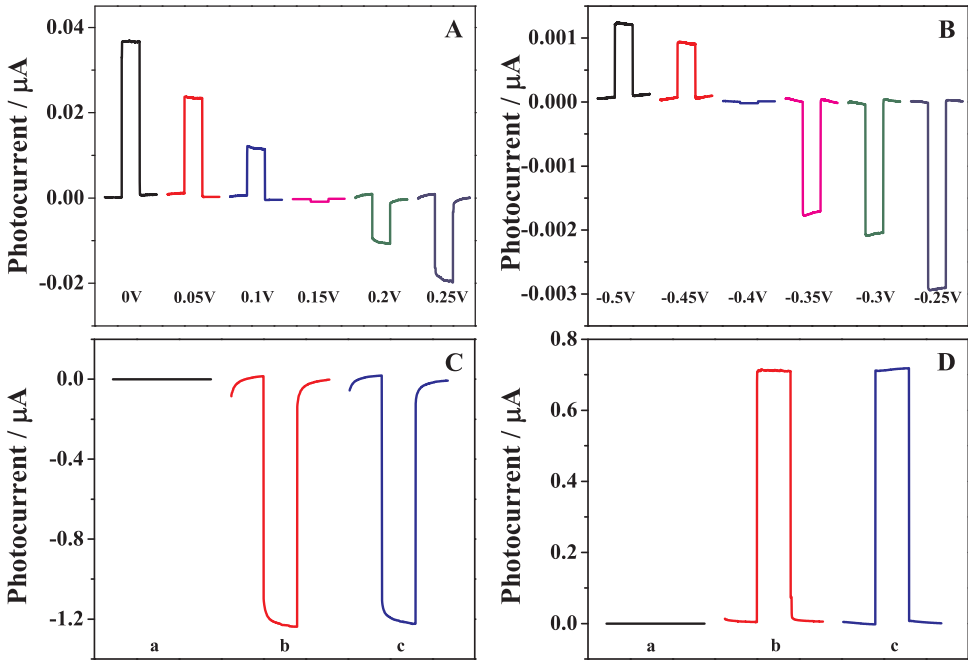

Fig. 3. Photocurrent of g-C_3N_4 (A) at 0 V, 0.05 V, 0.1 V, 0.15 V, 0.2 V, 0.25 V and C-dots/3DGH (B) at −0.5 V, −0.45 V, −0.4 V, −0.35 V, −0.3 V, −0.25 V; Photocurrent of (C) g-C_3N_4 (a), C-dots/3DGH (b) and g-C_3N_4 & C-dots/3DGH (c) at 0.15 V as well as (D) C-dots/3DGH (a), g-C_3N_4 (b) and g-C_3N_4 & C-dots/3DGH (c) at −0.4 V.

voltages of g-C_3N_4 and C-dots/3DGH were 0.15 V as well as −0.4 V, respectively. Therefore, as shown in Fig. 3C, when the voltage was set at 0.15 V, the photocurrent of g-C_3N_4 was zero (a) and C-dots/3DGH has a strong cathodic photocurrent (b). When the two materials were modified on two adjacent areas of one ITO electrode, the photocurrent of this electrode at 0.15 V was almost the same as the single C-dots/3DGH modified electrode (c). As shown in Fig. 3D, when the bias voltage was set as −0.4 V (the critical voltage of C-dots/3DGH), the photocurrent of the modified electrode of two materials (c) was also the same as g-C_3N_4 (b). As can be seen from above, the photocurrent from two materials could be clearly distinguished by changing the bias voltage.

Based on this principle, we designed the potentiometric resolved ratiometric PEC sensor for the detection of *E. coli*. In addition, the anti-interference ability of this sensor was investigated (Fig. 4). The photocurrent is very sensitive to the change of light intensity. However, the light intensity may fluctuate in a long-term PEC detection, resulting in positive or negative errors. The anodic photocurrent of g-C_3N_4 and the cathodic photocurrent of C-dots/3DGH at the corresponding bias potential increased significantly with light intensity increased from 25% to 100% (Fig. 4A). But the ratio of these two photocurrent intensity was basically stable, regardless of how the light intensity changed (Fig. 4B). Similarly, the effects of buffer solutions with different ionic strengths on photocurrents were also investigated (Fig. 4C and D), it could be found that the ratio of cathodic photocurrent to anodic current was much more stable compared with single photocurrent. The above experimental results showed that the designed ratiometric PEC sensor can effectively reduce the environmental interferences. (Hao et al., 2017b)

Fig. 5A represented photocurrents of g-C_3N_4 and C-dots/3DGH dual modified electrode in the presence of 2.9, 29, 2.9 × 10^2, 2.9 × 10^3, 2.9 × 10^4, 2.9 × 10^5, 2.9 × 10^6 cfu/mL *E. coli*. When increasing the concentration of *E. coli*, the cathodic photocurrent gradually decreased because of aptamer binding with *E. coli* and covering on the electrode surface. However, the anodic photocurrent did not change with the variation of concentration. As shown in Fig. 5B, the ratiometric of the photocurrent responses decreased with the increased *E. coli* concentration from 2.9 cfu/mL to 2.9 × 10^6 cfu/mL and the ratiometrics of I (cathodic photocurrent at 0.15 V) to I_0 (anodic photocurrent at −0.4 V) were proportionable to the logarithmic values of target concentrations. Owing to the saturation of target capture on the electrode surface, the rising of the photocurrent at higher concentration of *E. coli* gradually became slow.

3.5. Stability, repeatability and reproducibility studies

In Fig. S5A, dual modified ITO electrode was stored for one month, the photocurrent intensity of the electrode (b) was slightly lower than before (a) at 0.15 V bias potential, but it remained 96% of the original photocurrent value. Likewise, the photocurrent value of the electrode (b) also returned to about 96% of the initial (a) at −0.4 V bias potential (Fig. S5B). This phenomenon indicated that the sensor had an excellent stability.

In addition, the reproducibility of the photocurrent responses of g-C_3N_4 and C-dots/3DGH have been tested with different working electrodes. The photocurrent responses of g-C_3N_4 & C-dots/3DGH dual modified ITO electrodes at −0.4 V and 0.15 V, which show good reproducibility for six electrodes with consistent sensor surface area (Fig. S6A). The RSD_1 (the relative standard deviation of the photocurrent responses C-dots/3DGH) of 1.2% and the RSD_2 (the relative standard deviation of g-C_3N_4) of 3.2% were obtained. The repeatability of g-C_3N_4 & C-dots/3DGH dual modified ITO electrode was also examined. As shown in Fig. S6B, the responses of the same electrode after five consecutive operations under the same conditions were studied. The RSD_1 and RSD_2 were 3.2% and 2.8%, respectively, which means a good repeatability. Similarly, the reproducibility of photocurrent responses of g-C_3N_4 & C-dots/3DGH dual modified ITO electrodes before and after target detection at −0.4 V and 0.15 V were also investigated (by using six working electrodes with constant sensor surface area). It indicated that the potentiometric resolved ratiometric PEC aptasensor has good reproducibility before (Fig. S7A) and after (Fig. S7B) target detection. In Fig. S7 A, the RSD_1 of 1.9% and the RSD_2 of 2.6% were achieved. At the same time, the RSD_1 of 3.1% and the RSD_2 of 1.9% were also obtained from Fig. S7B.

3.6. Real sample analysis

The proposed method was applied in the real sample analysis to further investigate the practicality. The recovery test was examined by standard addition method, different concentrations of *E. coli* were added into 10-fold-diluted milk samples. As shown in Table S1, the

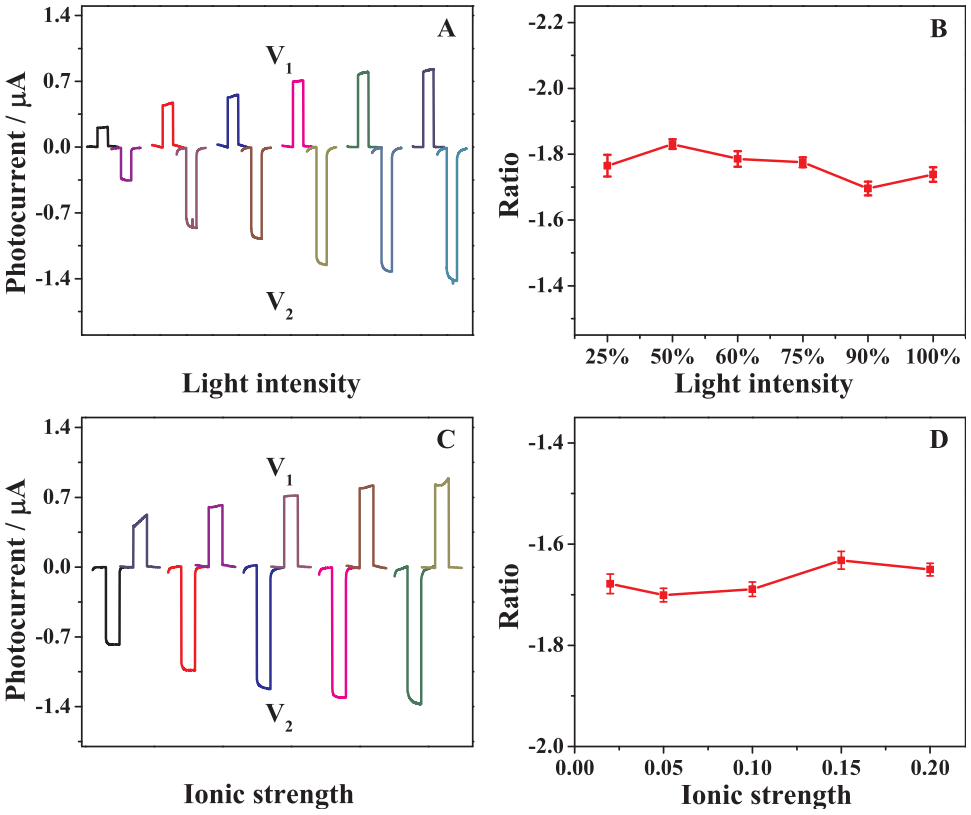

Fig. 4. Photocurrents of g-C_3N_4 & C-dots/3DGH dual modified ITO electrodes at different light intensity (A) and ionic strength (C) at −0.4 V (V_1) and 0.15 V (V_2) from left to right. Ratios of photocurrents at different light intensities (B) and ionic strengths (D) at −0.4 V (V_1) and 0.15 V (V_2).

recovery rate was found to be in the range of 98.6–102.0%, which indicated that the proposed method has a good stability. In addition, the developed method has a better sensitivity compared with traditional detection methods (Table S2).

4. Conclusions

For traditional PEC biosensors, the quantification of targets relies on the single photocurrent change, which is easily interfered by the environmental factors. In this work, a sensitive ratiometric PEC biosensor for *E. coli* detection was successfully developed with C-dots/3DGH and g-C_3N_4. These two nanomaterials were prepared with a facile method and avoided the use of precious metals or heavy metals, which is more environmental friendly and can reduce the potential toxicity. More importantly, based on the potentiometric resolved photocurrents, the concentration information may be obtained through the ratio of the cathodic current generated by C-dots/3DGH and the anodic current generated by g-C_3N_4. This strategy can effectively reduce the external factors interference and provide more reliable analysis performances. Meanwhile, this ratiometric PEC biosensor also showed a wide linear range (2.9 cfu/mL to 2.9 × 10^6 cfu/mL) and a good sensitivity (0.66 cfu/mL). This PEC biosensor didn't require additional instruments and can be widely applied, which would be potentially attractive for many related fields.

Acknowledgments

This work was supported by National Natural Science Foundation of China (Nos. 21505055, 21675066 and 21375044), Natural Science Foundation of Jiangsu Province (No. BK20150486), China Postdoctoral Science Foundation funded project (2017M621652), Postdoctoral Science Foundation funded project of Jiangsu province (1701075C), Foundation of Jiangsu University (15JDG145), Project Funded by the Priority Academic Program Development of Jiangsu Higher Education Institutions (No. PAPD-2014-37), Qing Lan Project. Zhenjiang city Science and Technology Support Program (Modern agriculture) project

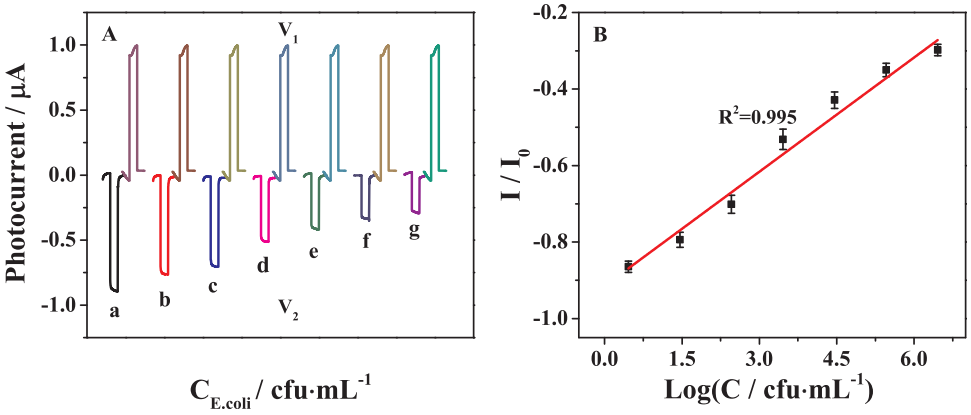

Fig. 5. (A) Photocurrents of g-C_3N_4 & C-dots/3DGH in the presence of 2.9, 29, 2.9×10^2, 2.9×10^3, 2.9×10^4, 2.9×10^5, 2.9×10^6 cfu/mL *E. coli* at −0.4 V (V_1) and 0.15 V (V_2), respectively. (B) Linear calibration curve of the ratios of I/I_0. (I was the photocurrent at 0.15 V and I_0 was the photocurrent at −0.4 V).

(NY2015015) and the Foundation of Key Laboratory of Sensor Analysis of Tumor Marker, Ministry of Education, Qingdao University of Science and Technology (No. SATM201807).

Appendix A. Supporting information

Supplementary data associated with this article can be found in the online version at http://dx.doi.org/10.1016/j.bios.2018.01.053.

References

Amiri, M., Salehniya, H., Habibi Yangjeh, A., 2016. Ind. Eng. Chem. Res. 55, 8114–8122.
Amouzadeh Tabrizi, M., Shamsipur, M., Saber, R., Sarkar, S., Ebrahimi, V., 2017. Biosens. Bioelectron. 98 (Suppl. C), 113–118.
Deisingh, A.K., Thompson, M., 2004. J. Appl. Microbiol. 96, 419–429.
Feng, Q.M., Shen, Y.Z., Li, M.X., Zhang, Z.L., Zhao, W., Xu, J.J., Chen, H.Y., 2016. Anal. Chem. 88, 937–944.
Gilje, S., Han, S., Wang, M., Wang, K.L., Kaner, R.B., 2007. Nano Lett. 7, 3394–3398.
Golub, E., Pelossof, G., Freeman, R., Zhang, H., Willner, I., 2009. Anal. Chem. 81, 9291–9298.
Han, D.M., Jiang, L.Y., Tang, W.Y., Xu, J.J., Chen, H.Y., 2015. Electrochem. Commun. 51 (Suppl. C), 72–75.
Hao, N., Zhang, X., Zhou, Z., Hua, R., Zhang, Y., Liu, Q., Qian, J., Li, H., Wang, K., 2017a. Biosens. Bioelectron. 97, 377–383.
Hao, N., Zhang, X., Zhou, Z., Qian, J., Liu, Q., Chen, S., Zhang, Y., Wang, K., 2017b. Sens. Actuators, B 250 (Suppl. C), 476–483.
Hussein, L.A., Magdy, N., Yamani, H.Z., 2017. Sens. Actuators, B. 247, 436–444.
Kang, Z., Jiao, K., Xu, X., Peng, R., Jiao, S., Hu, Z., 2017. Biosens. Bioelectron. 96, 367–372.
Lawal, D., Burgess, C., McCabe, E., Whyte, P., Duffy, G., 2015. J. Microbiol. Methods 114 (Suppl. C), 9–15.
Li, H., Li, J., Yang, Z., Xu, Q., Hu, X., 2011. Anal. Chem. 83, 5290–5295.
Li, H., Xiao, Q., Lv, J., Lei, Q., Huang, Y., 2017. Anal. Biochem. 531 (Suppl. C), 48–55.
Li, H., Qiao, Y., Li, J., Fang, H., Fan, D., Wang, W., 2016a. Biosens. Bioelectron. 77, 378–384.
Li, L., Zhang, Y., Zhang, L., Ge, S., Liu, H., Ren, N., Yan, M., Yu, J., 2016b. Anal. Chem. 88, 5369–5377.
Lin, Z., Xiong, X., Zheng, J., Wang, G., Yang, C., 2017. Mater. Lett. 202, 123–126.
Moakhar, R.S., Goh, G.K.L., Dolati, A., Ghorbani, M., 2015. Electrochem. Commun. 61, 110–113.
Qian, Z., Bai, H.J., Wang, G.L., Xu, J.J., Chen, H.Y., 2010. Biosens. Bioelectron. 25, 2045–2050.
Settu, K., Liu, J.T., Chen, C.J., Tsai, J.Z., 2017. Anal. Biochem. 534 (Suppl. C), 99–107.
She, X., Liu, L., Ji, H., Mo, Z., Li, Y., Huang, L., Du, D., Xu, H., Li, H., 2016. Appl. Catal. B 187, 144–153.
Siegmund, L., Burmester, A., Fischer, M.S., Wöstemeyer, J., 2013. Eur. J. Protistol. 49, 552–563.
Tan, C., Cao, X., Wu, X.J., He, Q., Yang, J., Zhang, X., Chen, J., Zhao, W., Han, S., Nam, G.H., Sindoro, M., Zhang, H., 2017. Chem. Rev. 117, 6225–6331.
Tiwari, S.K., Huczko, A., Oraon, R., De Adhikari, A., Nayak, G.C., 2017. Arab. J. Chem. 10, 556–565.
Wang, G., Xu, J., Chen, H., 2009. Sci. China Ser. B. 52, 1789–1800.
Wang, Y.Z., Hao, N., Feng, Q.M., Shi, H.W., Xu, J.J., Chen, H.Y., 2016. Biosens. Bioelectron. 77, 76–82.
Xu, X., Liu, D., Luo, L., Li, L., Wang, K., You, T., 2017. Sens. Actuators B 251, 564–571.
Yogesh, G.K., Shuaib, E.P., Sastikumar, D., 2017. Mater. Res. Bull. 91, 220–226.
Zhang, K., Zhou, H., Mei, Q., Wang, S., Guan, G., Liu, R., Zhang, J., Zhang, Z., 2011. J. Am. Chem. Soc. 133, 8424–8427.
Zhang, X., Xiao, Y., Qian, X., 2008. Angew. Chem. Int. Ed. 47, 8025–8029.
Zhang, Y., Hao, N., Zhou, Z., Hua, R., Qian, J., Liu, Q., Li, H., Wang, K., 2017. Chem. Commun. 53, 5810–5813.
Zhang, Y., Ma, H., Wu, D., Li, R., Wang, X., Wang, Y., Zhu, W., Wei, Q., Du, B., 2016. Biosens. Bioelectron. 77, 936–941.
Zhao, S., Li, Z., Li, Y., Yu, J., Liu, G., Liu, R., Yue, Z., 2017. J. Photochem. Photobiol. A 342, 15–24.
Zhao, W.W., Xiong, M., Li, X.R., Xu, J.J., Chen, H.Y., 2014. Electrochem. Commun. 38 (Suppl. C), 40–43.
Zhao, W.W., Xu, J.J., Chen, H.Y., 2015. Chem. Soc. Rev. 44, 729–741.
Zhu, D., Ren, A., He, X., Luo, Y., Duan, Z., Yan, X., Xiong, Y., Zhong, X., 2017. Sens. Actuators B 252, 134–141.
Zou, W., Shao, Y., Pu, Y., Luo, Y., Sun, J., Ma, K., Tang, C., Gao, F., Dong, L., 2017. Appl. Catal. B 218, 51–59.
Zhang, Y., Cui, W.Q., An, W.J., Liu, L., Liang, Y.H., Zhu, Y.F., 2018. Appl. Catal., B. 221 (Suppl. C), 36–46.